Hybrid density functional based study on the band structure of trioctahedral mica and its dependence on the variation of Fe^{2+} content

V. Timón [a],[*],[1], C.S. Praveen [b],[1], E. Escamilla-Roa [c], M. Valant [b]

[a] InstitutoAndaluz de Ciencias de la Tierra, Campus de Fuentenueva s/n, 18002 Granada, Spain
[b] Materials Research Laboratory, University of Nova Gorica, Vipavska 11C, 5270 Ajdovscina, Slovenia
[c] Instituto de Astrofísica de Andalucía CSIC, Granada 18008, Spain

ABSTRACT

A hybrid density functional based study of a phyllosilicate (PS) is presented here for the first time. Using all-electron electronic structure calculations with the B3LYP hybrid functional, we have investigated the electronic and structural properties of a series of trioctahedral 1M-polytype K-bearing micas starting from phlogopite (the Mg-end member), ending with the annite (the Fe-end member), and passing through the biotite (a solid solution of the end members). Electronic band gap is calculated for all the compositions and nature of the electronic transition is discussed with the aid of band structure and density of states plots. An excellent agreement with the available experimental data has been observed. An insulator to semiconductor transition is explained on the basis of orbital hybridization. A further comparison is made using the pure GGA functional. For the completeness of the study, the dielectric properties of phlogopite are calculated using the coupled perturbed Kohn–Sham scheme, as implemented within the CRYSTAL09 code.

© 2013 Elsevier Inc. All rights reserved.

1. Introduction

Electrical resistivity studies of the Earth's crust and upper mantle has a long history of several decades and interesting behaviors like the low resistance zones of the lower crust ('anomalous crustal conductivities') are still being debated [1]. This research could get further support by considering the electronic structure calculations over the main constituents of Earth crust and upper mantle such as clays, in particular, they being essential component of Earth's surface that form tiny nanocrystalline particles.

Clay minerals are layer-type aluminosilicates, referred to as phyllosilicates. The structures of phyllosilicates consist of two-dimensional layers of polyhedral (tetrahedral and octahedral) networks. The tetrahedral sheets are composed of SiO$_4$ tetrahedra, which are linked together by sharing three of the four vertices. Silicon as well can be substituted by other cations, for instance Al, thereby producing a different series of minerals [2]. The tetrahedral sheets are linked in the unit structure to the XO$_4$ (OH)$_2$ (X = Al^{3+}, Mg^{2+}, Fe^{3+} and Fe^{2+}) octahedral sheets. A wide range of minerals also exists with other type of cations in the octahedral sheet [3].

Depending on the octahedral site occupancy, two groups of phyllosilicates may arise: namely, the trioctahedral series (full cation octahedral occupancy, with divalent cation, like Mg^{2+} or Fe^{2+} and trivalent Fe^{3+}) and the dioctahedral series (where two out of three octahedra are filled with trivalent cations like Al^{3+} or Fe^{3+}) respectively [2]. In both series the different charged cations result in charged layers, which have to be compensated by large interlayer cations such as K$^+$, Na$^+$, Ca^{2+}.

Among the numerous families of phyllosilicates, the group formed by micas have a high interlayer charge (>1.8 charges per unit cell layer). Usually, a vast majority of micas are formed from magma (a rock-forming mineral, mainly found in all three rock types: igneous, metamorphic and sedimentary, respectively). Micas have an excellent insulator behavior and are widely used in industry [4]. However, they may alter their electrical properties and acquire conductivity by specific isomorphous substitution of cations such as Fe or Ti [5]. This insulator–conductor transition in some biotites upon isomorphous cationic substitution has been found experimentally. In 1968 Davidson and Yolfe [6] showed that the electrical conductivity in mica is a bulk-controlled process related to the presence of transition metals, wherein the transition metal cation, iron or titanium, alters the electronic behavior hence showing DC electronic conductivity. Moreover, in order to understand the thermal and structural evolution of oceanic lithosphere, it is very important to study the electrical conductivity [7,8] of its main component such as biotite phyllosilicates; in particular,

* Corresponding author. Tel.: +34 915616800.
E-mail addresses: vicentetimon@ugr.es, vtimon@iact.ugr-csic.es (V. Timón).
[1] These authors contributed equally.

phlogopite (the magnesium end member). Not only the conductivity but also the magnetism in micas showed intriguing behavior. Annite, the theoretical iron end-member of the trioctahedral biotite mica series as was described before, can form solid solutions with phlogopite. The octahedral sheet of Fe^{2+} magnetic ions is diluted by diamagnetic Mg^{2+}, while OH^- hydroxyl octahedral groups can be replaced by F^-. These substitutions, made in the solid solution series, allow systematic studies of 2D magnetism with site disorder, bond disorder, and combined site and bond disorder on the same hexagonal lattice as was studied by Rancourt et al. [9].

Much earlier attempts to calculate the electronic properties of these micas have been reported. For instance, the conductivity in biotite mica and the influence of composition on it is reported by Meunier et al. [5] and a further detailed study on the conductivity of trioctahedral iron vermiculite was reported by Rüscher et al. [10,11]. However, the experimental characterization of these micas is rather difficult due to the complexity of their crystal structures. Recently Rüscher [12] has described the fundamental electronic excitations such as small-polaron hopping depending on temperature in biotite micas. In silico theoretical studies are therefore highly desirable to aid the scarce experimental measurements.

Here we present the results of a systematic large scale density functional theory (DFT) based simulation of these materials starting with phlogopite, the magnesium end member. This is then followed by the analysis of the successive replacement of the octahedral Mg^{2+} cation by Fe^{2+} (biotite) until the $Fe^{2+/3+}$ end member configuration (annite) is obtained. Due to the low symmetry of the system, much computational effort (thanks to the HPC-Europa2 project) has been employed to attain a better spin polarized electronic description of these micas.

These complex materials are challenging for standard Kohn–Sham DFT approaches. In particular, it is well known that the traditional local-density approximation (LDA) and the semi-local generalized extensions (GGA) lead to a systematic underestimation of the quasi-particle band gap of semiconductors and insulators, the so-called band-gap problem [13]. In fact, there is no rigorous foundation to identify the one-particle KS eigenvalues of the *noninteracting* reference system of electrons which is defined within the KS formulation with the electron addition or removal energies of the real interacting system. In contrast, Koopmans' theorem relates the Hartree–Fock (HF) eigenvalues to them but the neglect of electronic correlation grossly overestimates the band gap. During recent years, it has been shown that the systematic underestimation of the band gap in DFT can be corrected by incorporating a fraction of single-determinant exchange within the hybrid DFT/HF approaches [14]. In particular, the reliability of

the popular B3LYP hybrid functional to determine band gaps has been proved for a wide range of materials (e.g., [15,16]) showing that this approach survives the "band gap problem" to a reasonable extent. To the best of our knowledge, a hybrid functional approach such as B3LYP is applied here for the first time to describe the electronic properties of a phyllosilicate.

The next section provides an outline of the computational and methodological details of our work along with a characterization of the adopted structural models. This is then followed by the description and discussion of the results on the structural and electronic properties of the phlogopite mica, as well as the effect of increasing the Fe^{2+} content on them. The results are mainly discussed on the basis of the band structure and density of states obtained with the spin polarized B3LYP functional. Section three closes with a summary of the results and future prospects.

2. Structural models and computational details

2.1. Structural models

Phlogopite and biotite micas are a common 2:1 layered phyllosilicate within the mica group described by the ideal formula $K_2(Mg_{1-x}Fe_x)_6 [Al_2Si_6O_{20}] (OH)_4$ where usually $0 < x < 0.6$ [10]. They are formed by a layer of octahedral magnesium oxy-hydroxides sandwiched between alternating layers of tetrahedral silicates. These three layers are covalently bounded together through common oxygen atoms, forming a layer structured repeating unit. The phlogopite is a hydrated phyllosilicate of potassium and magnesium, while the biotite is a solid solution between the magnesium end member (phlogopite: $[KMg_3AlSi_3O_{10}(OH)_2]$) and the iron end member (annite: $[KFe_3AlSi_3O_{10}(OH)_2]$ – mainly composed of Fe^{2+} but it can also contain Fe^{3+} to a smaller extend). In this work, different models of trioctahedral phyllosilicates with varying compositions are studied (Table 1). Starting from the magnesium end member, phlogopite, we successively substituted Mg^{2+} by Fe^{2+} to get the Fe-bearing biotite compositions. Finally, the iron end member annite was studied by filling the complete octahedral layer by Fe^{2+} atoms.

2.2. Computational details

Quantum mechanical calculations with GGA exchange functional and Becke's three-parameter hybrid functional B3LYP [17,18] were performed by using the ab-initio periodic program CRYSTAL [19,20] here the Kohn–Sham orbitals are expanded in local Gaussian-type orbitals (GTO). All-electron

Table 1
Calculated crystal parameters (distances in Å and angles in degrees), and electronic band gap (in eV) for all the seven studied systems.

Trioctahedral mica structure: structural formulae	a	b	c	α	β	γ	Vol Å³	band-gap (eV)
PS0 [$Mg_6(Si_6 Al_2)O_{20}(OH)_4K_2$]								
CRYSTAL	5.27	9.12	10.34	90.0	100.4	90.0	488.75	7.86
SIESTA	5.31	9.21	10.07	90.0	99.9	90.0	485.14	4.86
Experimental[a]	5.32	9.21	10.24	90.0	100.0	90.0	494.10	7.85–9.92[b]
Experimental[c]	5.36	9.29	10.41	90.0	100.0	90.0	510.48	
PS1 [(Mg_5Fe_1)($Si_7 Al_1$)$O_{20}(OH)_4K_2$]	5.27	9.14	10.35	90.2	100.3	90.0	490.91	4.02
PS2 [(Mg_4Fe_2)($Si_7 Al_1$)$O_{20}(OH)_4K_2$]	5.29	9.15	10.36	90.1	100.4	90.0	492.97	3.70
PS3 [(Mg_3Fe_3)($Si_7 Al_1$)$O_{20}(OH)_4K_2$]	5.29	9.17	10.37	90.1	100.5	90.0	494.84	3.54
PS4 [(Mg_2Fe_4)($Si_7 Al_1$)$O_{20}(OH)_4K_2$]	5.30	9.18	10.38	89.9	100.4	90.0	496.71	3.51
PS5 [(Mg_1Fe_5)($Si_7 Al_1$)$O_{20}(OH)_4K_2$]	5.31	9.22	10.32	89.9	99.7	90.7	498.36	3.50
Experimental[d]	5.33–5.40	9.22–9.35	10.29–10.32	90.0	99.1–100.0	90.0	≈495.00	
PS6 [(Fe_6)($Si_7 Al_1$)$O_{20}(OH)_4K_2$]	5.31	9.20	10.40	90.0	100.5	90.0	500.07	3.50
Experimental[e] (Annite)	5.37	9.31	10.28	90.0	100.2	90.0	505.25	

[a] From Reference [32].
[b] From Reference [46].
[c] From Reference [33].
[d] From Reference [45].
[e] From Reference [35].

(high-quality) basis sets, as available in the crystal website (www.crystal.unito.it/basis_sets/ptable.html), were adopted to span the Bloch orbitals of the crystals. They are denoted as H_3-1p1G, O_6-31d1, Al_85-11G*, Mg_8-511d1G, Si_88-31G*, K_86-511G, and Fe_86-411d41G. All calculations, including the geometry optimization, were carried out by using tight tolerance factors for the coulomb and single-determinant exchange series evaluation (referred to as ITOL values). The ITOLn (n = 1, 2, 3, 4, 5) tolerance parameters were set to 7, 7, 7, 7, 14, respectively (the meaning of these parameters is explained in Refs. [19,20]. The SCF convergence threshold was set to 10^{-8} ha. The reciprocal space was sampled according to a $4 \times 4 \times 4$ Monkhorst-Pack grid resulting in 36-k points in the irreducible part of the Brillouin zone. The DFT exchange correlation contributions were evaluated by a large internally predefined grid (a pruned grid composed by 75 radial and 434 angular points).

The unit cell parameters were optimized by keeping the atomic positions fixed. A further full relaxation of them was carried out for the samples describing phlogopite, biotite and annite, respectively. The relaxations were performed out by using a quasi-Newton optimization scheme as implemented in the CRYSTAL09 code. The detailed description of the method and the implementation is presented elsewhere [21–24]. The refractive index and the optical dielectric constants were calculated using the coupled perturbed Kohn–Sham scheme (CPKS) [25,26] while the static dielectric constants were obtained with a Berry phase approach [27].

For the sake of comparison with pure DFT methods and generalized gradient approximation (GGA), we also evaluated the electronic properties of the biotite crystal by using the orbital DFT code SIESTA [28,29]. The basis sets were composed by strictly localized numerical atomic orbitals (NAOs). The cutoff radii selected for the orbitals correspond to an energy shift of 250 Ry. The basis sizes were double-zeta polarized (DZP), following the perturbative polarization scheme. For all the model structures, both atomic positions and cell parameters were relaxed by means of conjugated gradient minimizations.

The graphics were performed by using the XCrySDen [30] program and the Material Studio (http://accelrys.com; 2005) package.

3. Results and discussion

Starting from phlogopite mineral, PS0 (c.f. Table 1), we first focused our attention in generating the most stable structures to compare with experimental results. Then we successively substituted Fe^{2+} atoms at the Mg^{2+} sub-lattice position. This is done in

this way up to the iron end member annite because in this structure the confirmed ratio of $Fe^{2+}:Fe^{3+}$ [31] is equal to 10:1 in octahedral coordination. However, the inclusion of such a small fraction of Fe^{3+} in our model will increase the size of the system remarkably and would require a supercell approach. Hence we limit our calculations only to Fe^{2+} content. Six such different configurations have been analyzed (PSn; n = 1, 2, 3, 4, 5, 6) as shown in Table 1. Due to the open shell occupation of the Fe-atom, spin polarized calculations were necessary to obtain accurate ground state energy. The energy difference between ferromagnetic and antiferromagnetic configurations is extremely small. For instance, in the case of sample PS2 the energy difference between the two configurations is as low as 0.02 eV. This falls within the error bar of the DFT calculations. Moreover, the difference in the value of the electronic band gap value is less than 0.1 eV. Thus, for brevity and ease of presentation we refer only to the ferromagnetic solutions. The geometry was optimized for each configuration in order to reduce the external pressure due to substitution. First we optimized the lattice parameters for all the structures by keeping the atomic coordinates fixed and later a full atomic coordinate relaxation have been performed for the end member samples (PS0 and PS6) and a biotite sample (PS2). Electronic band structure analysis, total orbital and atom projected density of states for the selected systems along with optical properties of phlogopite (PS0) are reported.

3.1. Structural properties

The phlogopite crystal belongs to the monoclinic space group $P_{2/1}$ with the local symmetry C_2^2. B3LYP-optimized lattice parameters along with available experimental data are collected in Table 1. As was described before, a full optimization of cell and atomic positions were done for PS0 to get a model that is a close description of phlogopite (Fig. 1). The results in all the biotite mica series are in good agreement with experimental data as seen from Table 1 [32–34] starting in phlogopite and finishing with the iron end member annite whose parameters agree also well with the experimental data [35].

As a result of the isomorphous substitution of divalent Mg^{2+} by Fe^{2+} in the octahedral sheet the unit cell edges b and c slightly increase. This elongation is also consistent with the progressive incorporation of Fe^{2+} into the octahedral sheet due to the larger ionic radius (0.77 Å) [36] compared to Mg^{2+} (0.72 Å) [37].

For a clear representation, in Fig. 2, we plotted the unit cell parameters b and c against the number of iron inside octahedral
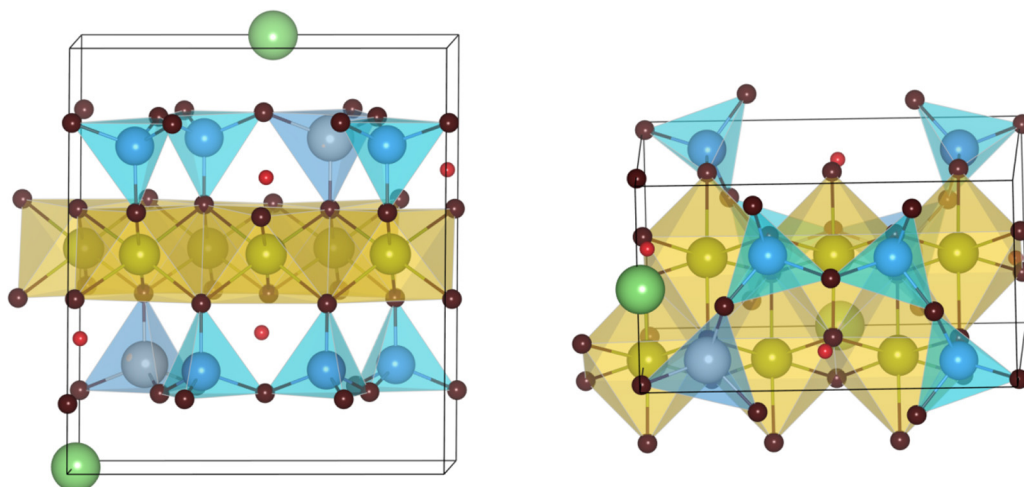

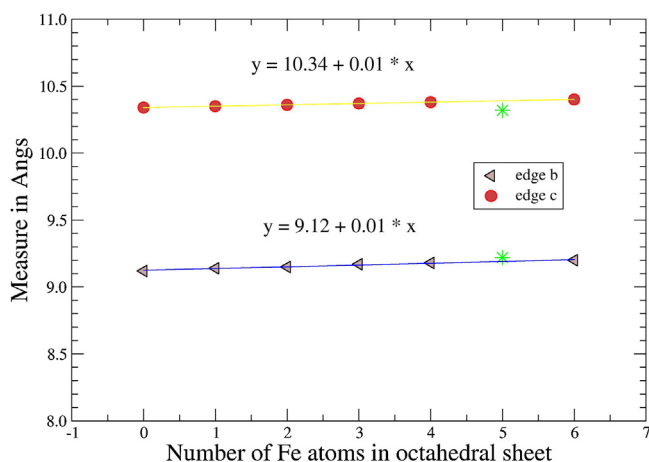**Fig. 1.** B3LYP optimized structure of phlogopite (PS0), biotite (PS2) and annite (PS6).

Fig. 2. Correlation between the iron content with respect to the **b** and **c** lattice parameters is plotted.

sheet. As seen from Fig. 2, it follows a good linear relationship as presented in Eqs. (1) and (2):

$$b = 9.12 + 0.013\,x; \quad R = 0.99 \tag{1}$$

$$c = 10.34 + 0.010x; \quad R = 0.99 \tag{2}$$

Here x is the number of Fe^{2+} atoms that substitute Mg^{2+} per unit cell.

Similar linear relationship has been observed (with slope 0.075) in octahedral isomorphous substitution of Al^{3+} by Fe^{3+} in other phyllosilicates such as nontronite [38] and kaolinite [39]. The values of the slope calculated from Eqs. (1) and (2), i.e. 0.013 and 0.010, are smaller than in nontronite and kaolinite. This can be attributed to the difference in radius, for instance in phlogopite mica, the difference in octahedral trivalent cation radius is 0.05 Å while in kaolinite it is 0.13 Å.

In the interlayer space the potassium is bound to the Si_5Al_1 ring with nearest K–O distances varying from 2.81 Å in sample PS0 to 2.86 Å in sample PS6. This deviation in bond enhancement suggests that charge localization on oxygen ions is directly connected to the substitution site in the octahedral layer [40]. Geometry considerations show some distortion from the ideal tetrahedral and octahedral configuration. Also, the T–O distances depends on the T – tetrahedral cation (Si^{4+} or Al^{3+}) – and octahedral M–O distance on change in M – octahedral (Mg^{2+} or Fe^{2+}) cation. In the phlogopite structure (PS0) the main T–T distances in tetrahedral hexagonal ring are between 3.00 and 3.06 Å, with T–T–T mean angles between 118.00° and 122.35°. Values are in a good agreement with distances and angles measured in phlogopite: 3.08 Å and 120° [41]. As the number of iron ions increases, the T–T distances increases slightly by a maximum of 0.02 Å per tetrahedral cation, while the angle remains equal.

The bond distances measured between the octahedral and tetrahedral sheets shows different behavior. The T–O distance between the tetrahedral silicon and octahedral oxygen, does not show any appreciable change with the iron substitution, keeping it nearly constant at 1.62 Å. While the T–O distance between the tetrahedral aluminum and octahedral oxygen changes from 1.71 to 1.74 Å as Fe^{2+} content increases. The T–O distance between tetrahedral cation and basal oxygen ions is approximately 1.76 Å for aluminum and 1.64 Å for silicon, which is in agreement with earlier reports [42]. We noticed that the octahedral M–O distance does not make any relevant changes in the geometry of the sheet. This might be so because the octahedra mainly reflect the topology of the tetrahedral, instead of the local crystal chemistry as observed in ferran tetra-ferriphlogopite [43].

For trioctahedral micas the OH group is forced to point directly into the interlayer site cavity as shown in Fig. 1. The increase of Fe^{2+} content results in a slight elongation of O—H bond length from 0.959 Å to 0.962 Å as same as in ferric dioctahedral micas [44].

3.2. Electronic structure analysis

The band gaps measured at the Γ-point single particle energy for structures from PS0 to PS6 are collected in Table 1. The B3LYP calculated values are in excellent agreement with the available experimental data as shown in the Table 1. For example the B3LYP calculated band gap value for the phlogopite is 7.86 eV which is very close to the experimental value of 7.85 eV [45,46]. The calculated band gap value with GGA (Becke) exchange using CRYSTAL is 5.58 eV. This value is underestimated by c.a. 30% compared to the experimental value. For a comparison we have calculated the GGA band gap using a norm conserving pseudopotential and local basis set with the SIESTA code and obtained the value 4.86 eV, which is again underestimated by almost 40%. Hence the importance in the selection of B3LYP functional at the all electron level in accurately predicting the band gap of micas is well demonstrated.

When the octahedral divalent cation Mg^{2+} is substituted by divalent Fe^{2+} cations, even if the net charge of the system remains constant, the electronic behavior changes substantially. The substituted Fe^{2+} ion introduce some mid band levels just above the top of the valence band and below the conduction band, thereby reducing the electronic band-gap. For example in the PS1 structure the electronic band gap is surprisingly reduces to 4.02 eV promoting an insulator to semiconductor transition. Further increase in the Fe^{2+} gradually reduces the band gap and saturates to a value of 3.50 eV, when all the Mg^{2+} is substituted by Fe^{2+}. This reduction in the band gap value is directly connected with the orbital hybridization. The interaction of O with the Mg atoms is covalent in nature, but is quite weak, at the same time O forms a very strong covalent bonding with the Fe atoms. The spin density analysis of the system further corroborates this assumption. The nominal atomic spin density at the Fe site is 3.7 μ_B, which is very low compared to the ideal value of 5. On the other hand a close observation of the spin density at the O-sites implies that there is an accumulation of charge at the O-sites at the nearest neighbor of the Fe atoms. For instance, there is a spin density of 0.1 μ_B is accumulated at the bridging oxygen between the two Fe sub-lattice positions in PS2 sample. While the spin density at the O-sites which are not connected with the Fe sub-lattice is nearly zero. Thus one could assume that there is a strong delocalization of charge from the Fe atom toward the O atom, thereby indicating a strong orbital hybridization between O-2p and Fe-3d (see below).

The up spin ("alpha") and down spin ("beta") band structure plots are shown along the high symmetric points of the first Brillouin zone for selected samples (PS0 and PS2) in Fig. 3. For the sake of clarity and ease of guidance, the total density of states is also plotted in Fig. 3 along with the band structure. The band structure of PS0 (Fig. 3a) and PS2 (Fig. 3b) is quite similar in the lower valence band and upper conduction band region. The valence band is highly entangled with majority of flat bands for PS0. While for PS2, in the valence band there appears localized bands both in the alpha and beta channels. The bands are very narrow with high density of states and are well separated from each other. This is because one of the t2g orbitals is doubly occupied and thus it has much lower energy. In sample PS2, the conduction band edge is again contributed by dispersion less narrow bands. For a detailed description of the nature of the bands, in Fig. 4, we have plotted the atom projected density of states of both PS0 and PS1 (PS2 is very similar except a much narrow gap) samples. As seen from Fig. 4a, it is clear that the top of the valence band of PS0 is mainly contributed by oxygen orbitals with a very small contribution from
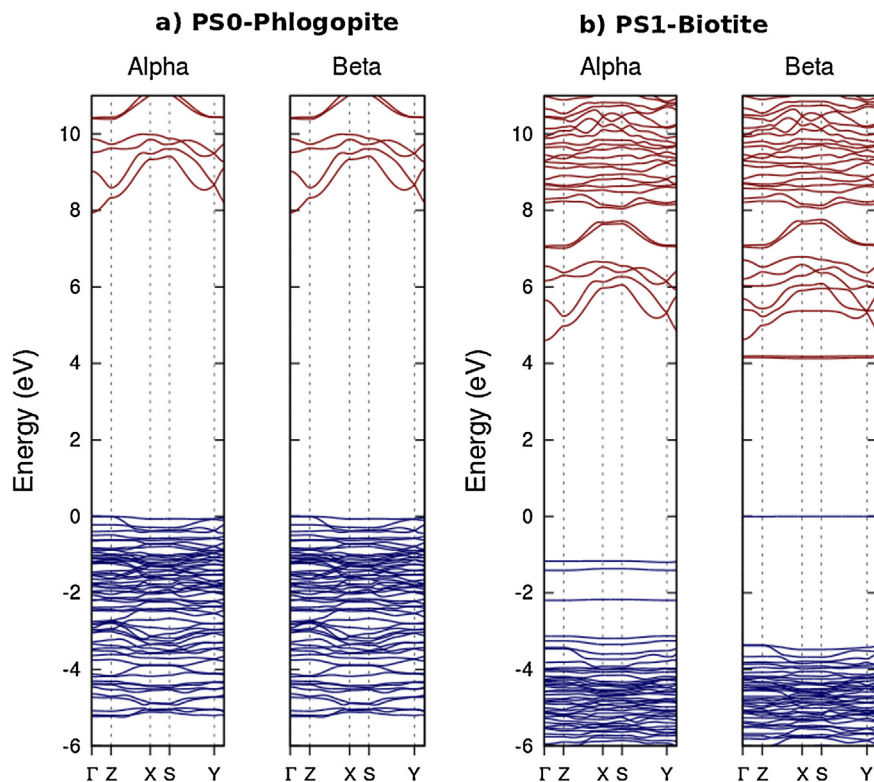
Fig. 3. B3LYP calculated band structure of phlogopite (PS0) and ferrous biotite (PS2). The total density of states is also plotted for ease of reference. Zero energy is taken as the top of the valence band for clarity.

silicon especially in the lower energy region. The contribution of all other atoms to the valence band is rather negligible. The bottom of the conduction band mainly comes from the hydrogen orbitals, while the upper conduction band has a higher contribution from the silicon orbitals. From Fig. 4b it can be inferred that the energy levels of oxygen and Fe atoms are nearly degenerate in the case of PS1 (see Fig. 6 for the case of PS2). Thus, the top of the valence band as well as the bottom of the conduction band is an admixture of Fe and O orbitals but the Fe contribution dominates. This can be again connected to the flatness of the bands at the band edges. Next to the Fe orbitals, there come two separated highly dispersed bands originating from the H and Si orbitals. These bands fall at the bottom of the conduction band in the case of the sample PS0.

Now in order to demonstrate the hybridization between the O-2p and Fe-3d orbitals, in Figs. 5 and 6, we have plotted the orbital projected density of states. In Fig. 5, the 2p levels of the O atoms that are close to the Mg atoms (a) and that are close to the Fe atoms (b) are plotted. It is clear from Fig. 6 that the oxygen atoms that are close to the Fe atoms fall at the same energy range of the Fe-3d orbitals. This results in a very strong hybridization between O-2p and Fe-3d orbitals as mentioned above and are responsible for an insulator to semiconductor transition.

For the completeness of the present study we also calculated the static and optical dielectric constants and the refractive index of phlogopite mica (PS0), which is reported in Table 2. We used the coupled perturbed Kohn–Sham scheme as implemented in the
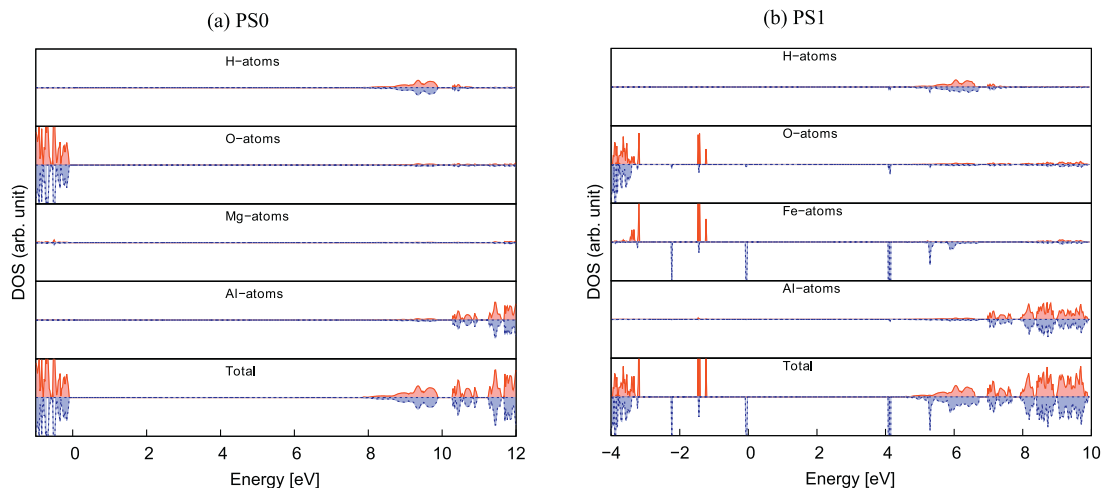

Fig. 4. Atom projected density of states of PS0 (a) and PS1 (b). The positive and negative values denote majority (red) and minority spin (blue) respectively. Zero (E–E_F) is taken as the top of the valence band.
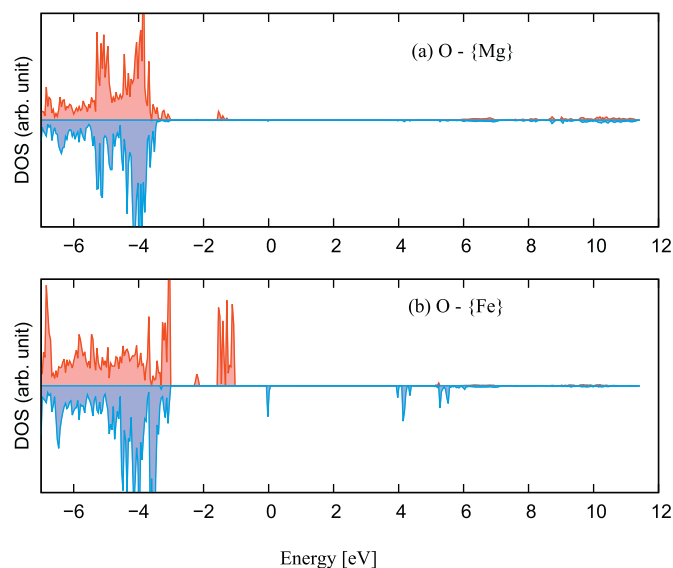
Fig. 5. Density of states of p-orbitals of the oxygen atoms which are bonded to Mg atom (a) and Fe atoms (b) for the sample PS2.
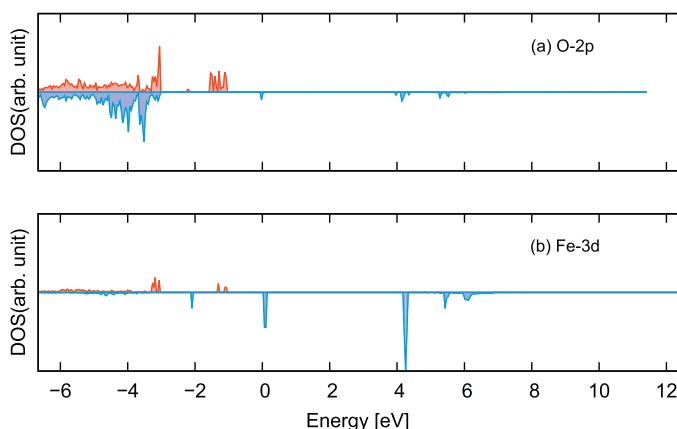

Fig. 6. Density of states projected onto the Fe-3d orbitals and O-2p orbitals close to the Fe atoms in sample PS2.

CRYSTAL code for the calculation of optical dielectric constant and refractive index, whereas the static dielectric constant is calculated with a Berry phase approach as available in the code. The results are in reasonable agreement with the available experimental data. The reported (293 K, 9.2 GHz) dielectric permittivity of phlogopite vary from 6.80 to 7.50 [47] while our calculated (0 K, no vibrational contribution) dielectric tensor values ranging from 4.74 to 6.31 are as well reported in Table 2.

Table 2
Static dielectric constant, optical dielectric constant and refractive index of phlogopite (PS0) calculated using CPKS scheme. Experimental data are provided in parenthesis.

Property	XX	YY	ZZ
Static dielectric constant (0 K) (experimental, 293 K[a])	6.12 (6.80–7.50)	6.31	4.74
Optical dielectric constant	2.08	2.09	1.41
Refractive index (experimental[b])	1.44 (1.52)	1.45 (1.55)	1.41 (1.55)

[a] From Reference [47].
[b] From Reference E.B.A. Bisdom, G. Stoops, et al. Micromorphology of weathering biotite and its secondary products, Pedologie 2 (1983) 225–252.

4. Conclusions

B3LYP hybrid functional, within the frame work of DFT, has been successfully applied to a series of trioctahedral 1M-polytype K-bearing trioctahedral micas starting from phlogopite (the Mg-end member), ending with the annite (the Fe-end member), and passing through the biotite (a solid solution of the end members). The calculated structural parameters are in good agreement with the available experimental data. The calculated electronic band gap (7.86 eV) shows an excellent agreement with the theoretical reports (7.85–9.92 eV). The biotite and annite structures were modeled by successive isomorphous substitution of divalent Mg^{2+} by Fe^{2+} in the octahedral sheet. As a result, the **b** and **c** lattice parameters increases and shows a linear relationship to the number of Fe content in the octahedral sheet similar to previous observations on nontronite and kaolinite. Regarding the electronic properties, the successive substitution of Fe in the place of Mg at the octahedral site brings an interesting insulator to conductor transition. This can be ascribed by a careful analysis on the electronic band structure. The Fe cation induces some mid band levels at above the valence and below the conduction band edges. This is the principle reason of the insulator to conductor transition. For the completeness of the present work optical and static dielectric constants of phlogopite together with refractive index is also reported. The reported values are in good agreement with the available data. In summary we have presented how efficient and practical is the hybrid functional approach in predicting the structural electronic and optical properties of complicated systems like phyllosilicates.

References

[1] G. Schwarz, Electrical conductivity of the earth's crust and upper mantle, Surveys in Geophysics 11 (2/3) (1990) 133–161.
[2] G. Brown, Crystal structure of clay minerals and related phyllosilicates, Philosophical Transactions of the Royal Society of London. Series A. Mathematical, Physical and Engineering Sciences 311 (1517) (1983) 221–240.
[3] D.M. Moore, R.C. Reynolds, X-Ray Diffraction and the Identification and Analysis of Clay Minerals, Oxford University Press, New York, 1997, pp. 378.
[4] A. Castellanos-Gomez, M. Wojtaszek, et al., Atomically thin mica flakes and their application as ultrathin insulating substrates for graphene, Small 7 (17) (2011) 2491–2497.
[5] M. Meunier, J.F. Currie, et al., Electrical conduction in biotite micas, Journal of Applied Physics 54 (2) (1983) 898–905.
[6] A.T. Davidson, A.D. Yoffe, Hopping electrical conduction and thermal breakdown in natural and synthetic mica, Physica Status Solidi (b) 30 (2) (1968) 741–754.
[7] A.M. Popov, A.I. Kiselev, et al., Geodynamical interpretation of crustal and upper mantle electrical conductivity anomalies in Sayan-Baikal province, Earth Planets and Space 51 (1999) 1079–1089.
[8] G. Heinson, S. Constable, The electrical conductivity of the oceanic upper mantle, Geophysical Journal International 110 (1) (1992) 159–179.
[9] D.G. Rancourt, I.A.D. Christie, et al., Magnetism of synthetic and natural annite mica: ground state and nature of excitations in an exchange-wise two-dimensional easy-plane ferromagnet with disorder, Journal of Magnetism and Magnetic Materials 138 (1/2) (1994) 31–44.
[10] C.H. Rüscher, S. Gall, Dielectric properties of iron-bearing trioctahedral phyllosilicates, Physics and Chemistry of Minerals 24 (1997) 365–373.
[11] C. Rüscher, S. Gall, On the polaron-mechanism in iron-bearing trioctahedral phyllosilicates: an investigation of the electrical and optical properties, Physics and Chemistry of Minerals 22 (7) (1995) 468–478.
[12] C.H. Rüscher, Temperature-dependent absorption of biotite: small-polaron hopping and other fundamental electronic excitations, European Journal of Mineralogy 24 (5) (2012) 817–822.
[13] A. Alkauskas, P. Broqvist, et al., Defect energy levels in density functional calculations: alignment and band gap problem, Physical Review Letters 101 (4) (2008) 046405.

[14] D.I. Bilc, R. Orlando, et al., Hybrid exchange-correlation functional for accurate prediction of the electronic and structural properties of ferroelectric oxides, Physical Review B 77 (16) (2008) 165107.

[15] J. Muscat, A. Wander, et al., On the prediction of band gaps from hybrid functional theory, Chemical Physics Letters 342 (3/4) (2001) 397–401.

[16] C. Di Valentin, A. Selloni, Bulk and surface polarons in photoexcited anatase TiO_2, Journal of Physical Chemistry Letters 2 (17) (2011) 2223–2228.

[17] A.D. Becke, Density-functional thermochemistry. III. The role of exact exchange, Journal of Chemical Physics 98 (1993) 5648–5653.

[18] A.D. Becke, A new mixing of Hartree–Fock and local density-functional theories, Journal of Chemical Physics 98 (2) (1993) 1372–1377.

[19] R. Dovesi, R. Orlando, et al., CRYSTAL: a computational tool for the ab initio study of the electronic properties of crystals, Zeitschrift fur Kristallograhie 220 (5/6) (2005) 571–573.

[20] R. Dovesi, V.R. Saunders, et al., CRYSTAL09 User's Manual, University of Torino, Torino, 2009.

[21] C.M. Zicovich-Wilson, F. Pascale, et al., Calculation of the vibration frequencies of α-quartz: the effect of Hamiltonian and basis set, Journal of Computers and Chemistry 25 (15) (2004) 1873–1881.

[22] F. Pascale, C.M. Zicovich-Wilson, et al., The calculation of the vibrational frequencies of crystalline compounds and its implementation in the CRYSTAL code, Journal of Computers and Chemistry 25 (6) (2004) 888–897.

[23] L. Valenzano, Y. Noël, et al., Ab initio vibrational spectra and dielectric properties of carbonates: magnesite, calcite and dolomite, Theoretical Chemistry Accounts 117 (5/6) (2007) 991–1000.

[24] L. Valenzano, A. Meyer, et al., Quantum-mechanical ab initio simulation of the Raman and IR spectra of $Mn_3Al_2Si_3O_{12}$ spessartine, Physics and Chemistry of Minerals 36 (7) (2009) 415–420.

[25] M. Ferrero, M. Rerat, et al., Coupled perturbed Hartree–Fock for periodic systems: the role of symmetry and related computational aspects, Journal of Chemical Physics 128 (2008) 014110–014117.

[26] M. Ferrero, M. Rérat, et al., The calculation of static polarizabilities of 1-3D periodic compounds. the implementation in the crystal code, Journal of Computational Chemistry 29 (9) (2008) 1450–1459.

[27] C.M. Zicovich-Wilson, R. Dovesi, et al., A general method to obtain well localized Wannier functions for composite energy bands in LCAO periodic calculations, Journal of Chemical Physics 115 (2001) 9708–9718.

[28] E. Artacho, D. Sánchez-Portal, et al., Linear-scaling ab-initio calculations for large and complex systems, Physical Status Solidi B 215 (1) (1999) 809–817.

[29] E. Artacho, E. Anglada, et al., The SIESTA method; developments and applicability, Journal of Physics: Condensed Matter 20 (6) (2008) 064208.

[30] A. Kokalj, XCrySDen—a new program for displaying crystalline structures and electron densities, Journal of Molecular Graphics and Modelling 17 (3/4) (1999) 176–179.

[31] R.M. Hazen, C.W. Burnham, The crystal structures of one-layer phlogopite and annite, American Mineralogist 58 (1973) 11.

[32] S.B. Hendricks, M.E. Jefferson, Polymorphism of the micas with optical measurements, American Mineralogist 24 (1939) 729–771.

[33] H. Steinfink, Crystal structure of a trioctahedral mica: phlogopite, American Mineralogist 47 (1962) 886–889.

[34] F. Scordari, E. Schingaro, et al., Red micas from basal ignimbrites of Mt. Vulture (Italy): interlayer content appraisal by a multi-methodic approach, Physics and Chemistry of Minerals 35 (2008) 163–174.

[35] G.J. Redhammer, A. Beran, et al., Spectroscopic and structural properties of synthetic micas on the annite-siderophyllite binary: synthesis, crystal structure refinement, Mossbauer, and infrared spectroscopy, American Mineralogist 85 (3/4) (2000) 449–465.

[36] J.L. Robert, R.C. Maury, Natural occurrence of a (Fe, Mn, Mg) tetrasilicic potassium mica, Contributions to Mineralogy and Petrology 68 (1979) 117–123.

[37] A. Decarreau, O. Grauby, et al., The actual distribution of octahedral cations in 2:1 clay minerals: results from clay synthesis, Applied Clay Science 7 (1/3) (1992) 147–167.

[38] J.D. Russell, D.R. Clark, The effect of Fe-for-Si substitution on the b-dimension of nontronite, Clay Minerals 13 (1978) 133–136.

[39] I. Iriarte, S. Petit, et al., Synthesis of kaolinite with a high level of Fe^{3+} for Al substitution, Clays and Clay Minerals 53 (1) (2005) 1–10.

[40] M. Diaz, J.-L. Robert, et al., Far-infrared study of the influence of the octahedral sheet composition on the K^+-layer interactions in synthetic phlogopites, Clays and Clay Minerals 58 (2) (2010) 263–271.

[41] Y. Kuwahara, Comparison of the surface structure of the tetrahedral sheets of muscovite and phlogopite by AFM, Physics and Chemistry of Minerals 28 (1) (2001) 1–8.

[42] H. Takeda, J.D.H. Donnay, Trioctahedral one-layer micas. III. Crystal structure of a synthetic lithium fluormica, Acta Crystallographica 20 (5) (1966) 638–646.

[43] M.F. Brigatti, L. Medici, et al., Crystal chemistry of trioctahedral micas-1M from Alto Paranaíba Igneous Province, Southeastern Brazil, Canadian Mineralogist 39 (2001) 1333–1345.

[44] C.I. Sainz-Diaz, V. Timon, et al., Quantum Mechanical calculations of dioctahedral 2:1 phyllosilicates: effect of octahedral cation distributions in pyrophyllite, illite, and smectite, American Mineralogist 87 (2002) 958–965.

[45] D.R. Wones, Physical properties of synthetic biotites on the join phlogopitc-annite, American Mineralogist 48 (1963) 1300–1321.

[46] A.T. Davidson, A.F. Vickers, The optical properties of mica in the vacuum ultraviolet, Journal of Physics C: Solid State Physics 5 (8) (1972) 879.

[47] O.I. Gudkov, M.S. Metsik, Dielectric properties of mica at shf, Soviet Physics Journal 16 (1973) 664–667.